PNAS RESEARCH ARTICLE | IMMUNOLOGY AND INFLAMMATION OPEN ACCESS

Subclass-switched anti-spike IgG3 oligoclonal cocktails strongly enhance Fc-mediated opsonization

Arman Izadi[a], Arsema Hailu[a], Magdalena Godzwon[b], Sebastian Wrighton[a], Berit Olofsson[a], Tobias Schmidt[c,d], Anna Söderlund-Strand[e], Elizabeth Elder[f], Sofia Appelberg[g], Maria Valsjö[h], Olivia Larsson[h], Vidar Wendel-Hansen[i], Mats Ohlin[b,j], Wael Bahnan[a], and Pontus Nordenfelt[a,e,1]

Edited by Ian Wilson, The Scripps Research Institute, La Jolla, CA; received October 14, 2022; accepted March 14, 2023

Antibodies play a central role in the immune defense against SARS-CoV-2. Emerging evidence has shown that nonneutralizing antibodies are important for immune defense through Fc-mediated effector functions. Antibody subclass is known to affect downstream Fc function. However, whether the antibody subclass plays a role in anti-SARS-CoV-2 immunity remains unclear. Here, we subclass-switched eight human IgG1 anti-spike monoclonal antibodies (mAbs) to the IgG3 subclass by exchanging their constant domains. The IgG3 mAbs exhibited altered avidities to the spike protein and more potent Fc-mediated phagocytosis and complement activation than their IgG1 counterparts. Moreover, combining mAbs into oligoclonal cocktails led to enhanced Fc- and complement receptor-mediated phagocytosis, superior to even the most potent single IgG3 mAb when compared at equivalent concentrations. Finally, in an in vivo model, we show that opsonic mAbs of both subclasses can be protective against a SARS-CoV-2 infection, despite the antibodies being nonneutralizing. Our results suggest that opsonic IgG3 oligoclonal cocktails are a promising idea to explore for therapy against SARS-CoV-2, its emerging variants, and potentially other viruses.

Fc-mediated function | phagocytosis | subclass | affinity | oligoclonal

SARS-CoV-2 has caused millions of deaths worldwide since it first emerged in 2019 (1). Early in the pandemic monoclonal antibodies (mAbs) were successfully used as therapeutics (2). These antibodies disrupted the angiotensin-converting enzyme 2 (ACE2) receptor-spike receptor-binding domain (RBD) interaction, thus neutralizing the virus and protecting the host (3). Neutralizing antibodies against the SARS-CoV-2 spike protein constitute only a fraction of the antibody immune response add of which only a fraction also neutralize the many virus variants that emerge over time (4). We have previously shown that a nonneutralizing but opsonic mAb was equally protective as a neutralizing mAb in an infection model of SARS-CoV-2 infection (5). These findings are in line with other studies showing that Fc-effector functions are crucial for viral control (6, 7). Indeed, the protection granted by vaccines against mutated variants like Omicron can partly be explained by intact antibody Fc-effector functions directed against non-RBD sites or RBD sites not subjected to mutations (8).

Antibody class and subclass play a significant role in determining functional outcomes, especially in the context of Fc and complement receptor (CR)-mediated phagocytosis. The human IgG class has four subclasses defined by differences in the constant domains of the heavy chain (9). The constant domain has historically been considered independent of the variable domain and is responsible only for antibody effector functions. However, growing evidence with subclass-switched antibodies shows that the constant domain seems to influence the affinity to the target antigen (10). Nonetheless, the antibody subclass constant domain research has mainly focused on the affinity to Fc-receptors and complement activation. IgG1 and IgG3 are the most potent activators of Fc gamma receptors on immune cells, likely due to their high affinity to these receptors (11). IgG3 is also the most potent activator of the classical complement pathway, followed by IgG1, 2, and 4 (12, 13). In the case of HIV-1, IgG3 has a stronger opsonic ability compared to IgG1 and mediates stronger Fc-mediated phagocytosis of beads conjugated with the gp140 antigen; this is despite IgG3 and IgG1 anti-HIV antibodies having similar affinities to their targets (14). The difference in function is attributed to the more extended hinge region on IgG3, which grants its Fc-tail more spatial flexibility. In a related study, exchanging the IgG1 hinge with an IgG3 hinge enhanced intracellular immunity against adenovirus infection, supporting the flexibility hypothesis (15). The IgG subclass, therefore, is a determining factor in optimizing the immune function of mAbs against viral pathogens. Recently it was shown that subclass-switching to IgG3 can enhance the neutralization of SARS-CoV-2 (16). Several

Significance

Monoclonal antibodies have been widely used as a therapy for COVID-19. The focus thus far has been on neutralizing antibodies that block viral entry into host cells. However, a typical immune response mostly leads to antibodies that cannot neutralize but help clear the infection by promoting immune cell function through opsonization. The constant antibody domain determines its class and subclass and can directly influence immune effects. Here, we show that switching subclass can modulate the immune response against the SARS-CoV-2 virus. Further, we enhance antibody-mediated immune function by combining antibodies into cocktails. This study highlights how antibody subclass engineering and incorporating antibodies into cocktails can modulate the efficacy of antibodies as potential therapeutics against viral infections.

Author contributions: A.I., M.V., O.L., V.W.-H., M.O., W.B., and P.N. designed research; A.I., A.H., M.G., S.W., B.O., A.S.-S., M.V., and O.L. performed research; A.I., B.O., T.S., E.E., S.A., M.O., W.B., and P.N. contributed new reagents/analytic tools; A.I., A.H., M.G., S.W., T.S., A.S.-S., M.V., O.L., M.O., W.B., and P.N. analyzed data; and A.I., W.B., and P.N. wrote the paper.

Competing interest statement: The authors have patent filings to disclose, A.I., W.B., and P.N. have a patent pending on the mAbs described in this manuscript with Tanea Medical AB.

This article is a PNAS Direct Submission.

[1]To whom correspondence may be addressed. Email: pontus.nordenfelt@med.lu.se.

This article contains supporting information online at https://www.pnas.org/lookup/suppl/doi:10.1073/pnas.2217590120/-/DCSupplemental.

Published April 3, 2023.

aspects are still unknown, such as the effect of the IgG subclass on antibody affinity to the spike protein, its impact on complement activation, its relationship to subsequent Fc-mediated immune functions, and how combining various anti-spike antibodies may influence Fc-mediated antibody functions.

In this work, we show that subclass-switching anti-spike mAbs from IgG1 to IgG3 alters antibodies avidity to spike protein. We also demonstrate that IgG3-switched antibodies enhance both Fc- and CR-mediated phagocytosis. These improved effector functions did not correlate with the original B cell subclass. We show that an oligoclonal cocktail of IgG3 mAbs is more potent than even the best-performing monoclonals in both Fc- and CR-mediated phagocytosis. The results in this study highlight the functional benefit of subclass-switching antibodies to the IgG3 subclass and utilizing them in oligoclonal cocktails for enhancing immune potency. Finally, we confirm the importance of Fc-mediated function in an animal model of SARS-CoV-2 infection where we find that opsonic, nonneutralizing IgG1 and IgG3 mAbs are protective. Our work shows that oligoclonal IgG3 mAbs could be a candidate mAb therapy against SARS-CoV-2 and possibly other viral pathogens where potent Fc-effector functions are desirable.

Results

Switching the IgG1 Constant Domain to IgG3 Can Alter the Avidity for Spike Protein. Previously, we generated 10 reactive antibodies against the Wuhan spike protein of SARS-CoV-2 through the isolation of spike-reactive B cells followed by single-cell sequencing (5). All the spike-reactive clones were opsonic in vitro. These mAbs were produced in the IgG1 subclass irrespective of the original subclass of the patient's B cells. Using PCR and homologous recombination, we exchanged the subclass-specific domains of the heavy chain in the heavy chain expression plasmid. We successfully generated 8 new heavy chain plasmids containing the original variable heavy domain and the IgG3 constant domain gene. The IgG3 subclass has an extensive number of allotypes encoding for human IgG3 constant domain (9). The allotype used in this study was IGHG3*11 which, amongst other differences, contains a 62 amino acid long hinge (9). The heavy chain plasmids were used with the original light chain plasmid to produce the IgG3 mAbs by Expi293F cells (Fig. 1*A*).

To measure the binding avidity of our newly produced mAbs, we conjugated biotinylated spike protein to fluorescent streptavidin microsphere beads (1 μm) as a model for SARS-CoV-2 virions (5). We incubated the IgG1 and IgG3 mAbs with the spike beads before adding secondary fluorescent anti-Fab antibodies to detect IgG binding on the beads using flow cytometry as done previously (5) (Fig. 1*B*). The avidity is calculated by fitting a nonlinear regression model to the dose-binding data. We observed that of our 8 IgG3 antibodies, 6 had an equivalent avidity to their IgG1 counterparts (Fig. 1 *C* and *D*). However, there was a notable change for Ab57 where the IgG3 version exhibited an increase in avidity compared to the IgG1 parent (Fig. 1 *C* and *D*). Ab11, on the other hand, showed severely reduced binding to spike as an IgG3 antibody, while the IgG1 version retained high reactivity. It is important to point out the different clonal origins of Ab57 and Ab11. In vivo, these had evolved into IgG1 and IgG3, respectively. The information acquired from the sequencing of clone 11's IgG3 constant domain was incomplete. Thus, the clone's original allotype could not be determined. In both these cases, the original subclass (IgG3 for clone 11 and IgG1 for clone 57) bound with lower avidity to the spike protein than the subclass-switched mAb variants, which were IgG1 and IgG3, respectively (Fig. 1*D*).

To complement the flow cytometry-based binding data, we performed surface plasmon resonance (SPR) to study spike-mAb affinity in the context of the respective monovalent domains. For clones 11 to 81, we used the spike protein's RBD as an analyte, while we used the N-terminal domain (NTD) in the case of clone 94. These clones were shown to bind to these respective domains from previous work (5). Neither Ab11, Ab36, nor Ab57 could bind to the RBD in this experimental setup for either subclass. For Ab59, Ab66, Ab77, Ab81, and Ab94, we observed no differences in affinity (in terms of k_A and K_D) (*SI Appendix*, Fig. S2*A*), confirming the previous avidity data from the spike bead flow cytometry assay. To measure the binding of Ab11, Ab36, and Ab57, we performed a similar experiment but replaced RBD as a ligand with the intact spike protein expressed as the trimer. In alignment with our prior discoveries, Ab11 displayed reduced reactivity towards the spike protein when expressed as IgG3, exhibiting an over 25-fold decrease in apparent K_D. (Fig. 1 *E* and *F*). However, we could observe no difference between IgG1 and IgG3 for clone 36. Clone 57 did show a twofold difference in apparent K_D in this experimental setup (Fig. 1 *E* and *F*). For clone 57, there was a threefold increase in rate constant for IgG3, further reinforcing its higher avidity. Contrary to the change in apparent K_D, clone 11 has a 1.7-fold higher constant rate (k_A) in the IgG3 subclass. The trimeric nature of the Spike protein antigen offers substantial opportunities for avidity effects in the binding assay that negatively impact the accuracy of measurement of the rate constants and affinities. The large size of this antigen furthermore provides a diffusion barrier that may affect the measurements. Thus, the constant for the interactions involving the trimer should be interpreted with caution. Nonetheless, the SPR results confirmed our previous findings that the lab-made Ab11 (in the form of IgG1) and Ab57 (in the form of IgG3) exhibit a heightened affinity toward the spike protein compared to their original native subclasses.

We further validated our findings regarding Ab11 and Ab57 by coating ELISA plates with spike and testing mAb reactivity. The ELISA experiments revealed that Ab57 demonstrated a much stronger binding to spike when expressed as IgG3, resulting in a several-fold increase in signal compared to IgG1 (Fig. 1*G* and *SI Appendix*, Fig. S3*A*). Additionally, as expected, Ab11 IgG3 exhibited a weakened reactivity toward spike (Fig. 1*G* and *SI Appendix*, Fig. S3*A*), whereas the IgG1 version displayed robust reactivity. Combined, the three methods demonstrate that, for clones 36, 59, 66, 77, 81, and 94, exchanging the constant domain from IgG1 to IgG3 has no impact on their avidity towards the spike antigen. However, altering the constant domain for clones 11 and 57 led to a substantial change in avidity. In these two cases, the most effective binding subclass was not the original subclass obtained from the donor B cell, as the artificially generated subclass-switched antibodies exhibited a superior binding strength (Fig. 1 *C*–*G*).

IgG3 Is a More Potent Inducer of Fc-Mediated Phagocytosis Than IgG1. In our previous work, we used the THP-1 cell line to study how the IgG1 monoclonals promote Fc-mediated phagocytosis of spike beads (5). These findings correlated with protection in an animal model. Using a similar approach, we incubated opsonized spike-coated microsphere beads with THP-1 cells to measure Fc-mediated phagocytosis. Since the mAbs were discovered by baiting B cells with the original Wuhan-1 spike, we opted to use this antigen for our subsequent analysis. We stained the beads with a pH-sensitive dye (pHrodo green) to distinguish cell populations with internalized beads vs. those that are only associated with beads (Fig. 2*A*).

On average, the IgG3 mAbs increased the percentage of cells with internalized beads more than twofold compared to their IgG1

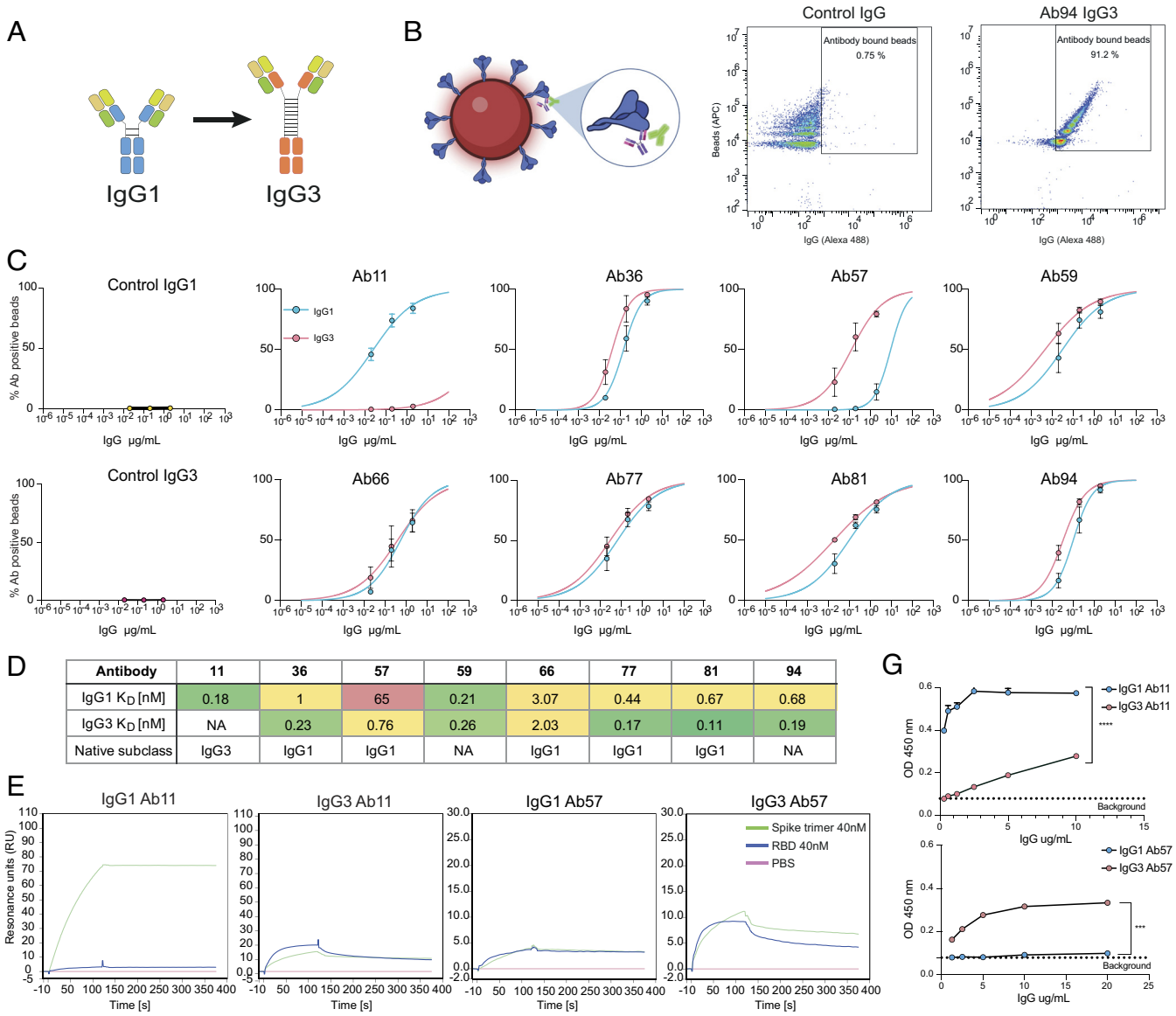

Antibody	11	36	57	59	66	77	81	94
IgG1 K_D [nM]	0.18	1	65	0.21	3.07	0.44	0.67	0.68
IgG3 K_D [nM]	NA	0.23	0.76	0.26	2.03	0.17	0.11	0.19
Native subclass	IgG3	IgG1	IgG1	NA	IgG1	IgG1	IgG1	NA

Antibody	11	36	57	59	66	77	81	94
IgG1 K_D(nM)	0.1	1.2	5.2	0.23	0.38	0.16	0.20	16
IgG3 K_D(nM)	2.6	1	2.2	0.21	0.47	0.15	0.14	19
IgG1 k_A ($M^{-1}S^{-1}$)	2.56E+05	1.18E+05	1.74E+05	1.30E+06	9.46E+05	1.58E+06	1.74E+06	7.83E+04
IgG3 k_A ($M^{-1}S^{-1}$)	4.36E+05	1.45E+05	5.06E+05	1.56E+06	1.02E+06	1.67E+06	1.95E+06	4.37E+04
Analyte	Spike	Spike	Spike	RBD	RBD	RBD	RBD	NTD

Fig. 1. Switching the IgG1 constant domain to IgG3 can alter the avidity for Spike protein. (*A*) Schematic of the heavy and light chain plasmids containing the variable and constant domains. The generation of IgG3 mAbs entails switching the constant domain of the heavy chain from IgG1 (blue) to IgG3 (orange). (*B*) Spike-coated microspheres are used as a model for SARS-CoV-2 virions. Antibody binding assay is done by opsonizing Spike beads with mAbs and adding a secondary Alexa 488-conjugated antibody that reports IgG binding to Spike beads. (*C*) Binding curves showing the percentage of IgG positive Spike beads as a function of IgG concentration. Each clone is shown with both subclasses present (IgG1 in blue and IgG3 in red). Three independent experiments were performed with the mean value shown in the graph and error bars representing the SEM. (*D*) Table summarizing the subclass K_D-values and original subclass for each clone. Avidity was calculated by using a nonlinear regression model in GraphPad Prism. (*E*) Surface plasmon resonance-based binding kinetics with whole spike protein (trimer). Binding of 40 nM Spike-protein (green) to immobilized IgG compared to 40nM RBD (blue) and PBS (pink) for clones 11, 36, and 57 and their respective subclasses. *F*) Table with KD-values and KA for the different subclasses across all clones (11 to 94) and what analyte (spike, RBD, or NTD) was used to measure it with the SPR-based assay. (*G*) ELISA data with spike-coated wells and bound IgG is shown for clones 11 and 57 and their respective subclasses. Three independent experiments were performed with titration curves to plot binding curves. Here, one representative experiment with 4 technical repeats is shown with mean value and error bars representing the SEM. Statistical analysis was performed using a two-tailed *t* test. *P* value above 0.05 denotes ns, *P* value below 0.05 denote *, *P* value below 0.01 denotes **, *P* value below 0.001 denotes ***, and *P* value below 0.0001 denotes ****.

counterparts. This was consistent across all mAb clones, except for Ab11 IgG3, reflecting its reduced avidity. The largest fold-change increase when switching from IgG1 to IgG3 was seen for Ab36 IgG3 (threefold) (Fig. 2*B*). In order of potency measured as % internalization, Ab94 (anti-NTD) IgG3 (47%) was the most potent, followed by Ab59 (38%) and Ab81 IgG3 (35%) (Fig. 2*B* and *SI Appendix*, Fig. S4*A*). To put these values into context, the most potent IgG1 antibody, Ab94 IgG1, was similar in potency to IgG3 Ab66 (17% vs. 20%), the second weakest IgG3 antibody in terms of internalization. IgG3 also led to an increased amount of opsonized beads associated with phagocytes compared to IgG1 (Fig. 2*C* and *SI Appendix*, Fig. S4*A*). This was seen as large differences in the median fluorescence intensity (MFI) signal of beads per cell. Ab94 IgG3 led to a sevenfold increase over Ab94 IgG1. Ab81 IgG3 led

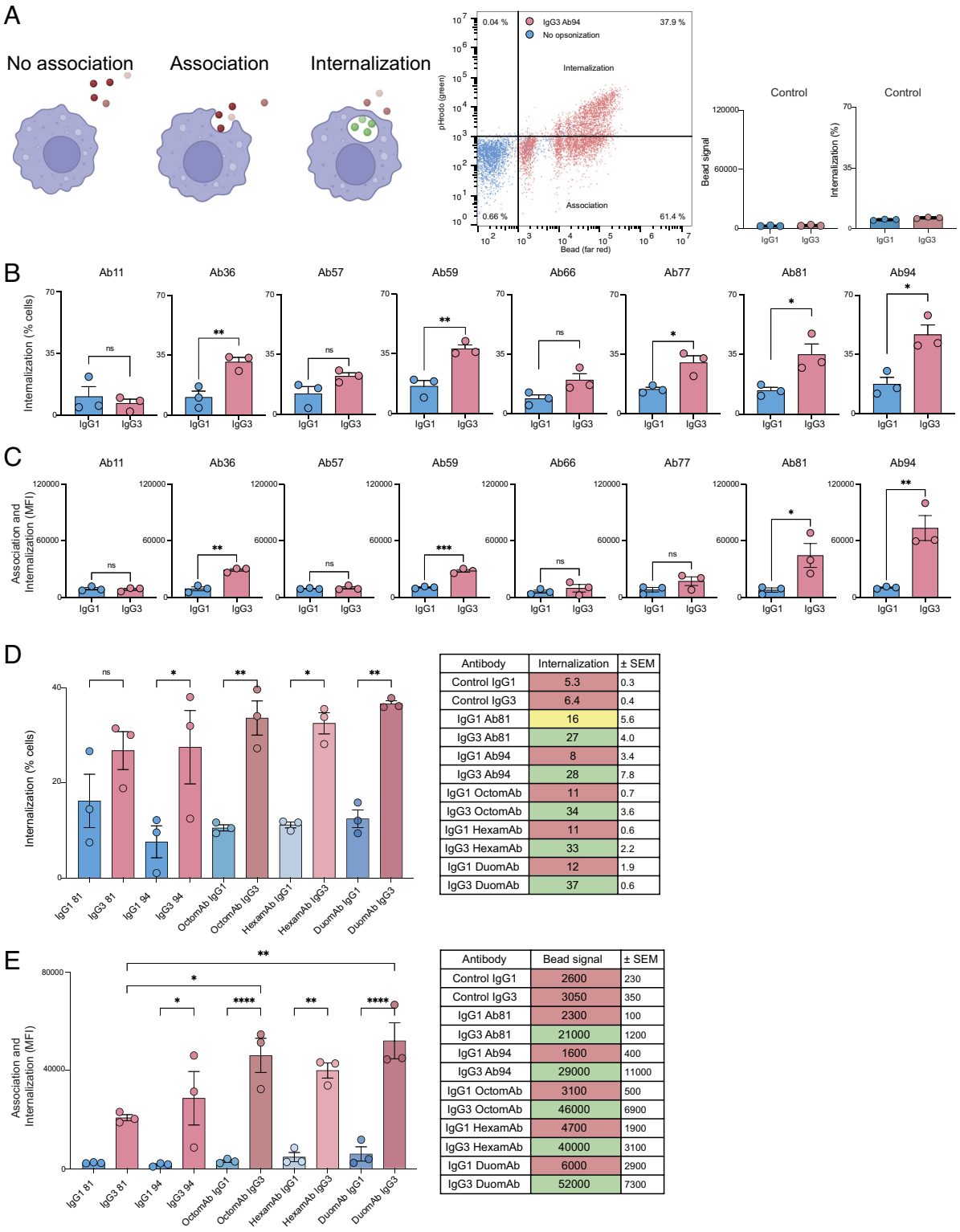

Antibody	Internalization	± SEM
Control IgG1	5.3	0.3
Control IgG3	6.4	0.4
IgG1 Ab81	16	5.6
IgG3 Ab81	27	4.0
IgG1 Ab94	8	3.4
IgG3 Ab94	28	7.8
IgG1 OctomAb	11	0.7
IgG3 OctomAb	34	3.6
IgG1 HexamAb	11	0.6
IgG3 HexamAb	33	2.2
IgG1 DuomAb	12	1.9
IgG3 DuomAb	37	0.6

Antibody	Bead signal	± SEM
Control IgG1	2600	230
Control IgG3	3050	350
IgG1 Ab81	2300	100
IgG3 Ab81	21000	1200
IgG1 Ab94	1600	400
IgG3 Ab94	29000	11000
IgG1 OctomAb	3100	500
IgG3 OctomAb	46000	6900
IgG1 HexamAb	4700	1900
IgG3 HexamAb	40000	3100
IgG1 DuomAb	6000	2900
IgG3 DuomAb	52000	7300

Fig. 2. IgG3 antibodies are superior to IgG1 antibodies at inducing Fc-mediated phagocytosis further potentiated when used as oligoclonal cocktails. (*A*) Illustration showing the three different phagocytic states cells can be in and how they are seen in flow cytometric gates: first depicting nonassociated cells, second associated but not internalized, and third with internalized beads. The gate to the right shows a double-positive population signifying internalized beads. Furthest to the right is a graph showing IgG isotype controls. *Y* axis shows the percentage of THP-1 cells with internalized beads. The same experimental conditions were used as in *B* and *C*. (*B*) IgG1 and IgG3 variants of each antibody clone mediate phagocytosis to varying degrees. The bar graph shows the percentage of cells with internalized beads. 10 μg/mL of the corresponding mAb was used to opsonize the beads (3 million beads per 100,000 phagocytes, a multiplicity of prey 30 (MOP 30). (*C*) Comparison between IgG1 and IgG3 for each clone with bead signal average for the whole THP-1 population. (*D*) The graph depicts how monoclonals compare to the cocktails in terms of bead quantity that is being phagocytosed by the whole cell population. The table to the right shows the mean values for the median bead signal (fluorescence intensity) for each treatment. (*E*) Comparison between IgG1 and IgG3 monoclonal antibodies and cocktails in terms of percentage of THP-1 cells with internalized beads. The table to the right summarizes the data from the graph with mean values from three experiments. In *D* and *E* 1.5 million beads per 100,000 phagocytes (MOP 15) were opsonized with 5 μg/mL of either monoclonal antibody or IgG cocktail. Statistical analysis was performed with a two-tailed *t* test in *B* and *C*. For *D* and *E*, statistical analysis was done with one-way ANOVA with multiple comparisons corrected with Tukey's test. *P* value below 0.05 is denoted by *, *P* value below 0.01 is denoted by **, and above 0.05 is denoted as ns. Three independent experiments were performed. Bars represent mean values, and error bars represent SEM. Three independent experiments were done for all experiments.

to a sixfold increase over its IgG1 counterpart, while no difference was observed for Ab11 and Ab57 IgG3. The difference between the IgG3 clones was much larger when analyzing MFI than the percent of phagocytes with internalized beads. Ab94 IgG3 led to far more beads being associated with the THP-1 cells (73000 MFI) compared to the other antibodies, followed by Ab81 IgG3 (44000). Again, the most potent IgG1 antibody, Ab59 (10500), was comparable to the weakest IgG3s (*SI Appendix*, Fig. S4*A*).

Our results show that the proportion of cells with internalized beads and the amount of beads associated with cells do not fully correlate, and each clone exhibits a unique pattern in these metrics. Ab59 IgG3 and Ab81 IgG3 were equivalent in promoting internalization of beads (38% vs. 35%). At the same time, Ab81 IgG3 also promoted a larger number of beads being taken up, seen as a higher bead signal (44,000 vs. 28,000). Similarly, while Ab36 IgG3 was similar to Ab77 IgG3 in terms of bead-internalizing cells (31% vs. 30%), there was a large difference in bead-signal (29,000 vs. 17,000). Moreover, Ab94 and Ab81 IgG3 stand out as the most potent mAbs in both metrics (Fig. 2 *B* and *C* and *SI Appendix*, Fig. S4*A*). Overall, exchanging constant domains to IgG3 enhances Fc-mediated phagocytosis for most of the tested mAb clones. Lastly, it is noteworthy to mention that the subclass-switched IgG3 forms of clones 36, 57, 66, 77, and 81, sourced from their donor B cells as IgG1s, demonstrated superior functionality compared to the original forms.

IgG3 Oligoclonal Cocktails Potentiate Fc-Mediated Phagocytosis Compared to Single Monoclonals. Although the monoclonal IgG3s show potent opsonic ability as single mAbs, a mAb-based experimental setup does not represent an in vivo setting. In blood, multiple antibody clones contribute to overall phagocytic performance. To emulate this, we created cocktails of all 8 mAbs called OctomAb. To observe the contribution of the most potent clones (Ab94 and Ab81 IgG3, antibodies that recognize two different domains of the spike protein), we created a cocktail consisting of these two mAbs named DuomAb. The remaining Ab11-Ab77 were put together in a third cocktail called HexamAb. We expected higher levels of bead signal and bead internalization when using cocktails. So as not to saturate the THP-1 cells, we lowered the multiplicity of prey (ratio of beads to phagocyte) from 30 to 15 and halved the concentration of mAbs (from 10 to 5 μg/mL).

The IgG3 cocktails clearly enhanced the phagocytic potency of the IgG3 mAbs. There was a threefold increase in the proportion of cells with internalized beads for all three cocktails compared to their respective IgG1 cocktails (Fig. 2*D*). HexamAb, which does not contain the potent Ab94 and Ab81 IgG3, achieved similar levels of phagocytosis as with monoclonal Ab94 IgG3 (32% vs. 27%). The observed differences were more pronounced (40,000 vs. 29,000, respectively) when looking at bead signals per cell (Fig. 2*E*). The IgG3 cocktails were much more potent in terms of the amount of associated beads per cell compared to their IgG1 counterparts. IgG3 DuomAb was eightfold more potent, HexamAb was 9-fold more potent, and OctomAb performed 12-fold better than IgG1 (Fig. 2*E*). Most importantly, all three cocktails exceeded the most potent IgG3 mAb (Ab94) with a 38% increase for HexamAb, 58% for OctomAb and 79% increase for DuomAb (Fig. 2*E*). Taken together, the results show that oligoclonal antibody cocktails, even with lesser-performing mAbs, promote potent phagocytosis exceeding the best-performing mAb at the same concentration.

IgG3 Monoclonals Activate Complement with High Potency Not Exhibited by Their IgG1 Counterparts. Next, we analyzed how well our IgG3 monoclonals and cocktails activate the classical complement pathway. We measured complement activation by adding 1% serum to opsonized spike beads. Using a secondary anti-C1q antibody (FITC), we could measure C1q deposition on the spike beads by flow cytometry (*SI Appendix*, Fig. S5). As clones 81 and 94 performed best in the previous assays, they were used as representatives for monoclonals. DuomAb and OctomAb cocktails were used to evaluate the benefit of cocktail use since these were the most potent cocktails. To avoid donor variability in terms of the presence of spike-reactive antibodies, we used pooled human serum depleted of antibodies as the source of complement.

The only mAb that by itself was able to induce C1q deposition was Ab94 IgG3 (Fig. 3 *A* and *B*). When using both Ab81 IgG3 and Ab94 IgG3 together as DuomAb, they deposited 2.5 times more C1q on the spike beads than Ab94 alone (38% vs. 15%, Fig. 3 *A* and *B*). This potent complement activation was not seen with IgG1 DuomAb, indicating that it is a subclass-dependent phenomenon. The OctomAb containing all antibodies triggered C1q deposition to a similar degree as DuomAb, but only its IgG3 form. We then performed C1q deposition analysis as a function of mAb concentration. We calculated the EC_{50} of DuomAb IgG3 and compared it to Ab94 IgG3. The resulting analysis shows that the addition of Ab81 IgG3 to Ab94 IgG3 increases the percentage of beads with C1q deposition more than threefold (EC_{50} decreased from 37 to 11 μg/mL, Fig. 3*C*). There was also a 20-fold increased deposition of C1q per bead (EC_{50} decreased from 230 to 15 μg/mL) (Fig. 3*D*). This meant that, compared to Ab94 alone, DuomAb led to a much stronger deposition of C1q on the beads. Combined, the results demonstrate a significant boost in the potency of anti-spike IgG3 mAbs compared to IgG1 in triggering the classical complement pathway, with the enhancement further amplified when utilizing the IgG3 mAbs in combination.

Fc-Mediated Phagocytosis of Spike-Coated Beads by Neutrophils Is Potentiated by IgG3 Monoclonals and Their Cocktails. We decided to validate our phagocytosis findings with primary immune cells. We first used monocytes to determine how the multiplicity of prey (MOP) would affect internalization, as this is an essential experimental factor to consider in phagocytosis (17). At low MOP (<1), monocytes barely internalize the spike beads, even with the potent OctomAb IgG3 (*SI Appendix*, Fig. S6*A*). However, at higher MOPs (1-10), the opsonic efficiency of mAbs is increased. To study the effects of IgG1 and IgG3 mAbs on primary cells, we therefore used a MOP of 5. We opted to use neutrophils instead of monocytes in subsequent experiments since they are more efficient at mediating phagocytosis and the most abundant phagocyte found in the blood (18).

The results show only a minor difference between heat-inactivated (HI) serum and complement-active (C+) treatments. This indicates that Fc-mediated phagocytosis is the dominating mode of function for anti-spike monoclonals of both subclasses and that complement-mediated phagocytosis plays a minor role (Fig. 3*E*). When comparing subclasses, all IgG3 treatments were superior to their IgG1 counterparts in the proportion of neutrophils with internalized beads (Fig. 3*E*). The IgG3 cocktails were, as seen previously, equal to or slightly better than Ab94 IgG3 by itself (C+: OctomAb: 15.0± 1.6%; DuomAb: 15.5± 1.1% and Ab94: 13.1± 2.9%) (Fig. 3*E*). OctomAb IgG1 (C+, 3.4± 0.3%) was slightly better than both Ab81 (C+,0.4± 0.1%) and Ab94 IgG1 (C+, 0.6± 0.1%) which was not seen with THP-1 cells previously (Fig. 2 *D* and *E*). However, a clear difference between OctomAb IgG1 and OctomAb IgG3 was seen again (3.4% vs. 15.0%).

We also studied the quantity of beads being phagocytosed by the cells. Due to the lower MOP (MOP 30 vs. 5), the neutrophils internalized less beads (%) compared to the THP-1 cells prior. We analyzed the bead signal for the bead-positive neutrophils

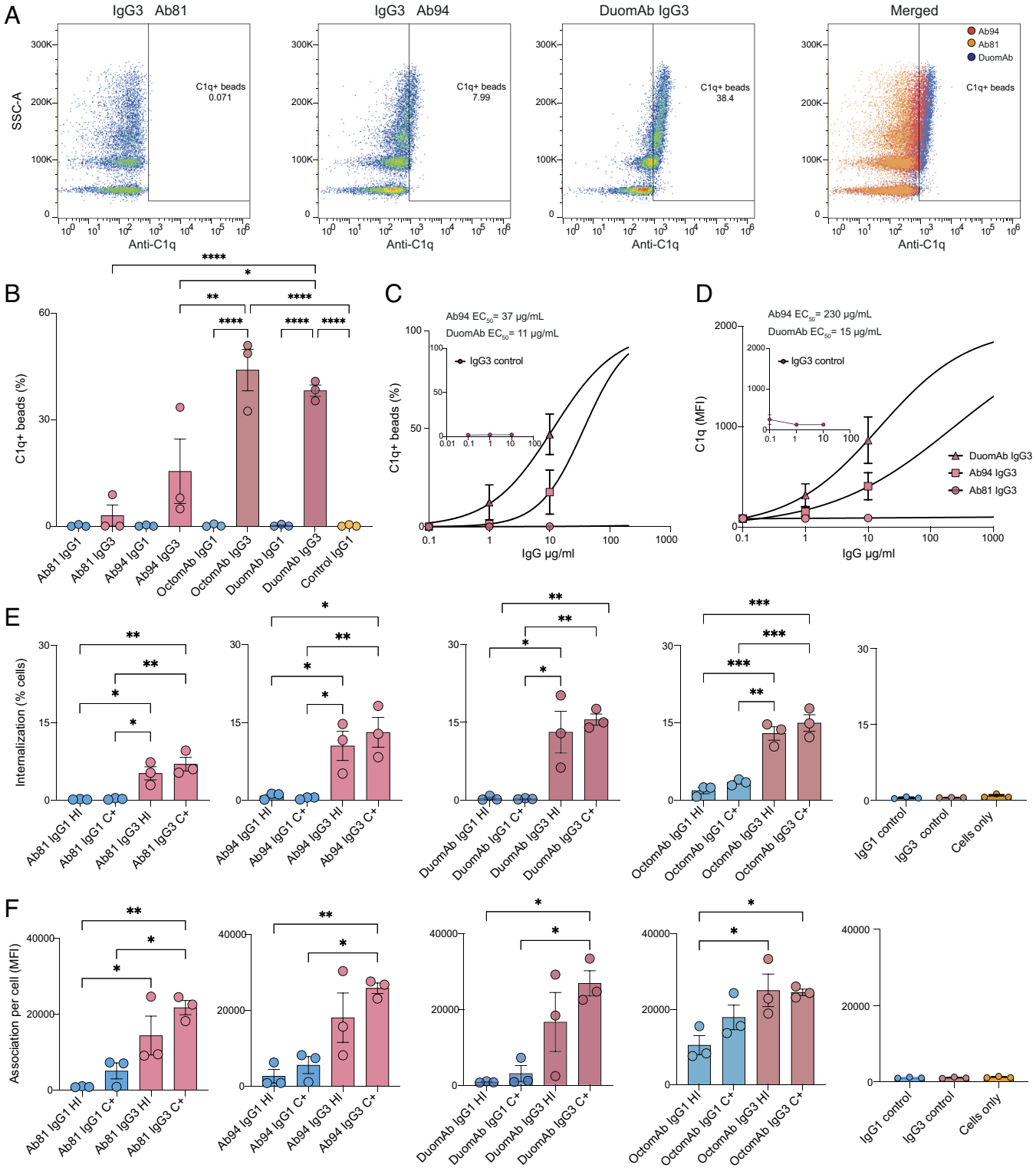

Fig. 3. IgG subclass and oligoclonality affect complement activation and phagocytosis of spike beads by neutrophils. (*A*) Individual gates for C1q deposition for Ab81, Ab94, and OctomAb IgG3 at 10 µg/mL. The far-right panel shows all three plots merged. (*B*) shows data on C1q deposition for the indicated monoclonals and oligoclonal cocktails. (*C*) Percentage of C1q deposition as a function of antibody concentration with EC_{50} values in the graph. (*D*) Fluorescent signal of deposited C1q as a function of antibody concentration with EC_{50} values present in the graph. In *C* and *D*, IgG3 isotype control data are shown as a small graph in each respective graph. (*E*) Neutrophils with internalized spike-beads comparing different treatments and heat-inactivated serum (HI) with complement-active serum (C+). (*F*) Bead signal of neutrophils associated with beads (APC+, *SI Appendix*, Fig. S2*D*). (*E* and *F*) Isotype controls are shown furthest to the right. Three independent experiments were performed for *A*–*E*. For *A*–*E*, statistical analysis was performed with one-way ANOVA and correction for multiple comparisons was done with Tukey's test. * denotes *P* value below 0.05, ** denotes *P* value below 0.01, *** denotes *P* value below 0.001, and ns denotes a *P* value above 0.05.

(APC+, *SI Appendix*, Fig. S6*B*). This analysis reveals that all IgG3 treatments remained superior to their IgG1 counterparts (Fig. 3*F*), as seen with THP-1 cells. Interestingly, IgG1 OctomAb showed enhanced phagocytosis compared to the single IgG1 monoclonals, which was not seen with THP-1 cells (Figs. 2*B* and 3*F*). This indicates that even IgG1 mAbs can benefit when used as cocktails to increase phagocytosis efficiency. Taken together, the results show that IgG3 monoclonals and their cocktails outperform their IgG1

counterparts in promoting phagocytosis (Fc- and CR-mediated). Both subclasses benefit from using a cocktail-based oligoclonal approach for enhancing phagocytic performance.

We utilized live fluorescence microscopy to study the temporal dynamics of the phagocytic process elicited by the mAbs. We focused on comparing the best monoclonal Ab94 IgG3 and the oligoclonal OctomAb in its IgG1 and IgG3 forms. We did not heat-inactivate the serum to also include CR-mediated phagocytosis. Since we wanted to compare the results with our flow cytometry data, we used neutrophils from the same donors (Fig. 3 *E* and *F*) and the same experimental conditions (MOP 5). We looked at neutrophils with internalized beads and quantified the percentage of these cells and the amount of beads they had internalized (Fig. 4*A*, images taken at experiment termination after 60 min). OctomAb IgG3 stands out among treatments by yielding more cells with internalized beads during the 60-min experiment (Movies S1–S4). We analyzed the potency of the IgG mAbs by calculating the time when 50% of all the neutrophils have internalized beads (ET_{50}). This analysis shows that OctomAb IgG3 promoted twice as fast internalization of spike beads compared to Ab94 IgG3 and OctomAb IgG1 (calculated ET_{50} of 35 min, 66, and 62 min, respectively) (Fig. 4*D*). All mAb treatments are more efficient than the untreated negative control (ET_{50} of 165 min, Fig. 4*D*). Still, only OctomAb IgG3 led to a statistically significant difference. Interestingly, OctomAb IgG1 and Ab94 IgG3 performed equally over time (Fig. 4*D*). This reaffirms the results in Fig. 3 *E* and *F*, where an IgG1 cocktail enhanced more weakly performing IgG1 mAbs. While we previously used the median bead signal to quantify how many beads were being phagocytosed, live imaging allowed us to do this with greater precision (Fig. 4*A*). The result from this analysis showed that cells with internalized beads have, on average, more beads internalized in each neutrophil when the opsonin is OctomAb IgG3 and Ab94 IgG3, compared to OctomAb IgG1 (Fig. 4 *B* and *C*). However, since OctomAb IgG3 activates more cells than Ab94 IgG3 (Fig. 4*D*) (72% vs. 47% after 60 min), it promotes stronger bead-cell interaction overall. Together, these results highlight the benefit of using an oligoclonal cocktail of mAbs to increase the efficacy of mAbs for both IgG1 and IgG3.

Opsonizing Anti-Spike mAbs Mediating Fc-Mediated Function Protects Against SARS-CoV-2 Infection. We next wanted to evaluate the biological and potential clinical relevance of the enhanced Fc-mediated functions we have observed with subclass-switching in protection against a true SARS-CoV-2 infection. The protective function of our mAbs was tested in an infection model using hACE2-K18 mice (Fig. 4*E*). We prophylactically injected each mouse intraperitoneally with a single dose (200 μg/mouse) of our mAbs (Ab94 IgG1, Ab94 IgG3, Ab81 IgG3, DuomAb IgG3 or vehicle control). Eight hours after mAb administration, we inoculated the mice intranasally with 1×10^5 PFU (SARS-CoV-2; Wuhan strain) of the virus. It is important to note that none of these antibody clones have neutralizing activity, as verified by three independent methods (5), and are considered strictly opsonic.

We theorized that all our antibodies would be protective compared to the vehicle control through their Fc-mediated effector functions. Measured daily over the experiment, mice given Ab94 IgG1 or Ab81 IgG3 showed lower weight loss compared to the vehicle control from days 0 to 7. More importantly, all the mAbs prevented death (mice were killed when experiencing >20% body weight loss) (Fig. 4*E*). On the seventh day, the mortality rate in the control group of mice was 100%, as opposed to the groups treated with mAbs (highlighted in Fig. 4*F* as survival *beyond* day 6 as a red dashed line). These data are also reflected in the state of the mice in terms of survival status and body weight at day 6 (Fig. 4*G*). On day 6, four out of six mice in the control group were deceased, and one mouse in the Ab94 IgG3 group had been killed (Fig. 4*G*). No mortality was observed in the other groups treated with the antibody, and the average weight remained within a healthy range (Fig. 4*H*). It is noteworthy that the only groups with survivors until day 10 were the Ab94 IgG1 and Ab81 IgG3 (Fig. 4*I*). After the mice were killed, irrespective of which day (ranging from day 5 to 10), bronchoalveolar lavage fluid (BAL) was harvested from the mice, and viral titers were analyzed by qPCR. The results are presented as cycle thresholds (CT). Whereby a higher value signifies a lower viral load. This analysis showed that the animals treated with all the mAbs, except DuomAb, had higher CT threshold values and, therefore, lower viral load upon killing (Fig. 4*J*). Ab94 IgG1 had the highest CT value (24.5), followed by Ab94 IgG3 (19) and then Ab81 IgG3 (18.1) compared to the control (17.8) (Fig. 4*J*). Our data shows that the mAb-treated mice had, in general, healthier mean weight, increased survival, and lower bronchial viral load. Taken together, our results show that opsonizing anti-spike antibodies, irrespective of the subclass, can be protective in a pre-clinical animal model of authentic SARS-CoV-2 infection. While Ab94 IgG1 performed the best in all aspects of the in vivo experiment, other antibody preparations, although overall better than vehicle control, were more variable in terms of measured treatment outcomes. Nevertheless, our data further adds to growing evidence (7, 19–22) that highlights the biological relevance of studying Fc-mediated effector functions in SARS-CoV-2 adaptive immunity. Like previous work (7, 19–22), our study shows that Fc-mediated functions can be protective against SARS-CoV-2 infection, especially in the context of nonneutralizing mAbs.

Discussion

The basis for mAb therapy against SARS-CoV-2 rested on the ability of neutralizing mAbs to bind to the RBD and disrupting the spike protein's ability to interact with the ACE2 receptor. Due to the rise of extensive mutations found in the RBD of the emerging variants of concern (VOC), most of the therapeutic antibodies isolated early during the pandemic lost binding, leading to loss of function and treatment failure (23, 24). This has led to alternative strategies such as combining a nonneutralizing antibody and a neutralizing antibody in a cocktail (22) or finding universally neutralizing antibodies to treat these new variants (25). An alternative strategy to consider would be to target epitopes for antibody therapy that do not rely on the spike RBD. Strong evidence emerging from animal models (6, 7, 19–21, 26) and patient material (8) suggests that Fc-mediated functions are important in the immune defense against SARS-CoV-2. The future of mAb therapies targeting SARS-CoV-2 would therefore benefit from optimizing Fc-effector potency through careful selection of the appropriate target epitopes, antibody subclass, and additional Fc-engineering.

In non-SARS-CoV-2 contexts, IgG3 mAbs have been shown to be efficient at mediating Fc-mediated phagocytosis of a bead-based model for HIV virions (14). A similar benefit has been observed with enhanced intracellular activity against an adenovirus via the TRIM21-receptor (15). In both these instances, the IgG3 hinge was thought to be responsible for this increased efficacy compared to other subclasses. This study focuses on how Fc-mediated immune functions of antibodies against spike protein can be potentiated. We find that altering the subclass leads to an increase in immune potency. Our data show that IgG3 versions of an array of spike-specific antibodies are superior in function in vitro to their IgG1 counterparts—even if they were originally derived from an IgG1 B cell. Moreover, our data show that

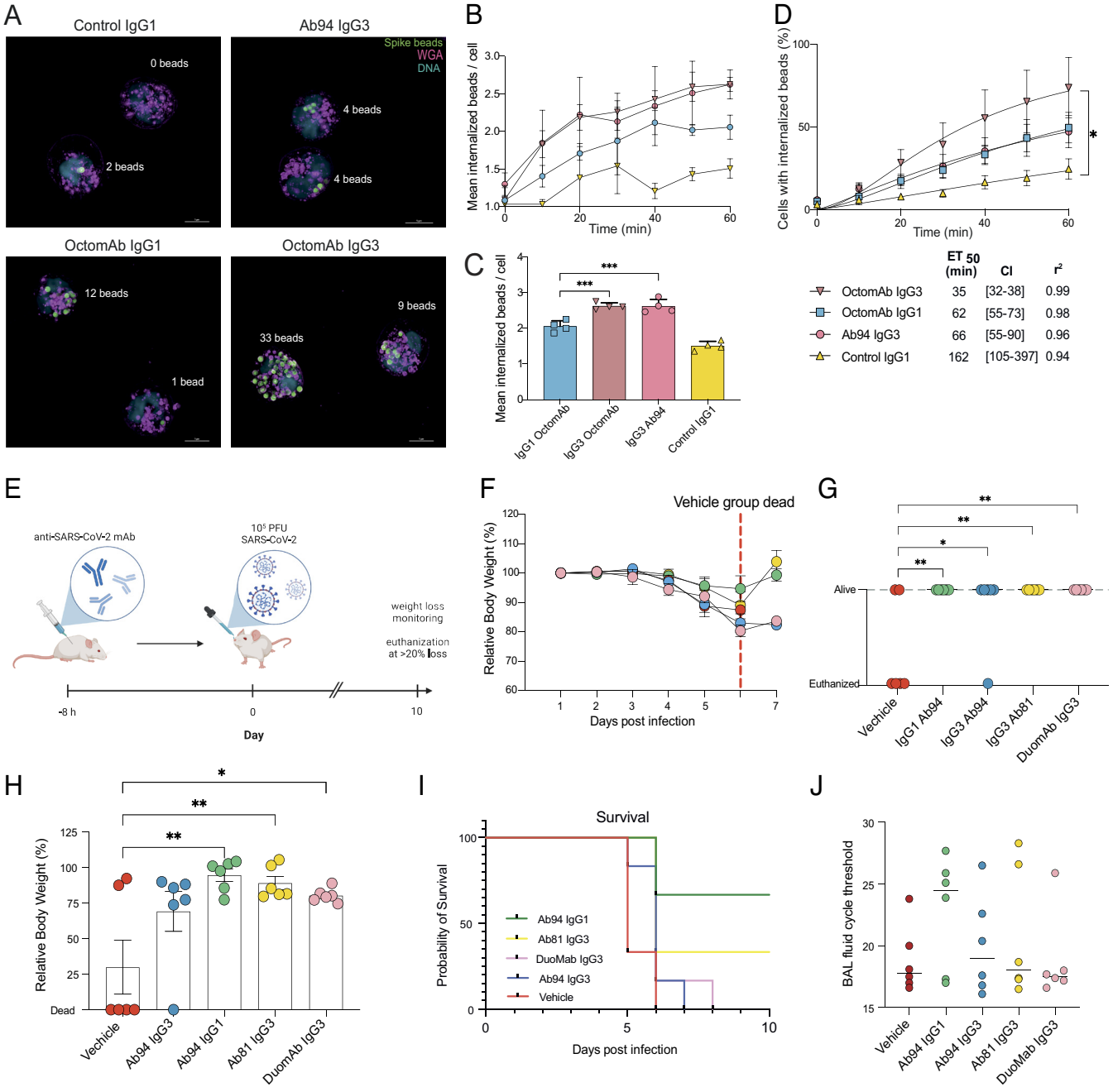

Fig. 4. Fc-mediated protection in vivo with hACE2-K18 mice and live imaging of human neutrophil phagocytosis. (*A*) Super-resolution structured illumination microscopy images showing human neutrophil phagocytosis of spike beads opsonized with indicated treatments. Beads are seen in green color in the picture (far red stain), cell surface in magenta (Alexa 594-WGA), and DNA in blue (Hoechst). pHrodo green was used as an internalization marker not seen in the image. Different antibody treatments result in differences in the number of beads internalized and the percentage of cells internalizing beads. SIM images are seen in a maximum-intensity projection of Z-stacks. Example images are shown from one experiment out of four. (Scale bars are 5 μm.) (*B*) Change in the average number of beads for the neutrophils with internalized beads over time. The bar graph in (*C*) shows the results after 60 min. (*D*) Temporal change in phagocytosis is monitored and displayed in terms of neutrophils with internalized spike beads. Below the graphs, ET_{50} values are presented in the table with 95% CIs in brackets. (*E*) Human ACE2-K18 mice were prophylactically injected intraperitoneally with antibody treatment or vehicle. Eight hours posttreatment, mice were infected intranasally with SARS-CoV-2 (Wuhan strain). Body weights were measured over 10 d. (*F*) Mean relative body weight for each group from days 0 to 7, the red dashed line highlights when all mice in the control group were deceased. (*G*) Status of each mouse (alive/killed) in each treatment group at day 6. (*H*) Relative body weight for each mouse in each treatment group at day 6, with killed mice set to 0. (*I*) Survival curves for each treatment group over the 10-d experiment. (*J*) Terminal titers of viral load were analyzed from BAL-fluid from mice that were killed, irrespective of which day of death. qPCR was done on BAL-fluid, and the cycle threshold was recorded and graphed. The median value is shown. The mean value is shown for figures *B–D* and *F–J*, with error bars being SEM. Statistical analysis was performed by one-way ANOVA, and correction for multiple comparisons was done with Tukey's test. * denotes *P* value below 0.05, ** denotes below 0.01, *** denotes below 0.001, **** denotes below 0.0001, and ns denotes *P* values above 0.05 and are not shown. In *B–D*, the data are from four independent experiments with four different donors.

Fc-mediated function is greatly enhanced when antibodies are combined into cocktails.

An incredibly large number of IgG antibody clones circulate in blood at any given time. Blood contains a versatile polyclonal mix of antibodies that become geared to antigen-specific antibodies after infection. In our current work, we show that in the hierarchy of efficacy, single IgG3 antibodies (e.g., Ab94) can be very efficient at mediating Fc-mediated immune function. However, when pooled together (Hexamab), multiple lesser efficacious antibodies can be equally potent in mediating immune

function. This could be due to enhanced Fc-receptor activation due to the clustering of multiple Fcs on the antigen trimer, theorized to be important for efficient phagocytosis (27–29). The findings regarding the importance of cocktails also translated into an increased efficacy in activating complement deposition.

C1q requires multiple Fcs formed into a hexamer to be activated (30). Our results suggest that IgG3 cocktails are more efficient at forming hexamer clusters than IgG1 cocktails. It is noteworthy that the cocktail's efficacy was more pronounced when used for opsonizing spike beads for neutrophils, compared to THP-1 cells. This could be attributed to neutrophils being professional phagocytes with a broader repertoire of phagocytic receptors (31). We have shown how we can potentiate immune function by combining multiple opsonic mAbs. We believe that considering an IgG3 platform for future mAb therapy against emerging VOCs and other pathogens could be a promising approach, as IgG3s are more functionally active in vitro than IgG1, especially in cocktail form.

IgG3 has inherent biological limitations to its utilization as a pharmaceutical agent in vivo, which are important to discuss. Of the four IgG subclasses, IgG3 has the shortest half-life (9) due to lower affinity to the neonatal Fc-receptor (9). However, the affinity to the Fc-neonatal receptor can be increased through Fc-engineering without diminishing Fc-effector functions (32, 33). This alteration has enhanced in vivo protection in a mouse model (30). We believe that one possibility of Ab94 IgG3's worse performance compared to its IgG1 counterpart could be explained due to its shorter half-life. Moreover, the half-life of human IgG is shorter in mice than in humans—on the order of days rather than weeks (34). Human IgG3, which already has a short half-life of 7 d (IGHG3*11), has an even lower half-life in mice. Human IgG3 has a sevenfold lower half-life in mouse blood (1 d), while human IgG1 has a fourfold lower half-life (5 d) (34). Therefore, over the 10-d experiment, the IgG3 mAbs would most likely have been eliminated to a further extent than IgG1 (34). It is worth noting that despite having a much lower half-life, Ab81 IgG3 was close to Ab94 IgG1 in protective effect. We believe this is because it has a higher affinity than both subclasses of clone 94, compensating for its low half-time (unlike Ab94 IgG3). Clone 81 is, therefore, a promising candidate in future projects if the IgG3 backbone's half-life is increased.

Besides the apparent pharmacokinetic differences mentioned above, major discrepancies in pharmacodynamic traits for human IgG1 and IgG3 exist when working with mice vs. human immune cells. Mice have different Fc-receptors expressed on their phagocytes compared to human phagocytes (35). Although these Fc-receptors have strikingly similar affinities to human subclasses as those seen in human Fc-receptors (36), they are understudied, especially in the context of IgG3 and its many allotypes. Studies of human subclasses investigating affinities to mouse Fc-gamma receptors have observed that human IgG3 binds as efficiently as IgG1. However, despite this, human IgG3 has been shown to have reduced in vitro function by mouse phagocytes compared to human IgG1 (37, 38). This is contrary to in vitro studies with human phagocytes, where human IgG3 has a more potent function than IgG1 (12–14, 32). Thus, due to the different pharmacokinetics and dynamics at play in this mouse model for human IgG subclasses, it is difficult to predict the outcome of these antibodies in a human context. The results need to be interpreted with caution. More work is needed to better link in vitro assays, in vivo animal models, and potential clinical benefits when studying human IgG subclasses as therapeutics. However, we believe the hACE2-K18 model is a good model for showing the biological relevance of Fc-effector functions against SARS-CoV-2 infections as a proof of concept. As long as human subclasses can mediate phagocytosis through mouse immune cells, the protective benefit of nonneutralizing mAbs can be studied in this model. Therefore, from the perspective of understanding the role of Fc-mediated function in SARS-CoV-2 immunity, our in vivo data shows that nonneutralizing antibodies can by themselves be protective against SARS-CoV-2 infection. However, not all nonneutralizing antibodies targeting the spike protein are necessarily protective. This is exemplified in a previous study where a nonneutralizing antibody was not protective by itself, and only when combined with a neutralizing antibody, protection was observed (22). Thus, we believe our proof-of-concept data, combined with other researchers' findings, highlights the importance of studying IgG Fc-effector response toward Sars-CoV-2. In this regard, generating human IgG3's remains a promising alternative to IgG1, especially if its pharmacokinetic traits with shorter half-life are addressed, and a different animal model is utilized in future studies oriented toward clinical application.

Finally, we present evidence that exchanging constant domains impacts the ability of the variable domain to bind to the spike protein. Ab11 IgG3 exhibits reduced avidity compared to Ab11 IgG1. Ab57 IgG3, on the other hand, binds better than IgG1. This is interesting because clone 57 was originally IgG1, and clone 11 was originally IgG3 (according to single-cell sequencing data) (5). An IgG1 antibody is formed when the IgG3 constant domain gene is deleted during the class-switch recombination process (9, 39). Thus, IgG1 can evolve from an IgG3, but an IgG3 cannot develop from a clone producing an IgG1 antibody. Although an IgM can be switched directly to an IgG1 antibody without having an IgG3 intermediate, a B cell that makes an IgG3 has not evolved to produce an IgG1. Interestingly, the artificial Ab11 IgG1 has a much higher avidity to spike than the original IgG3. In addition, Ab57 IgG3 shows that a theoretically less evolved mAb is more reactive to the antigen than the naturally evolved Ab57 IgG1. These examples raise the question if the most reactive mAb being expressed by a B cell is the one circulating in B cells at any given point at the 6 to 8 wk window postinfection [the patient's B cells were acquired 6 to 8 wk after initial SARS-CoV-2 infections (5)]. Our results show that the change of avidity does not always follow the anticipated subclass switch chronological hierarchy of the IGHV locus. However, our data are based only on eight clones but raise new questions which are worth considering. Our results further add to growing evidence (10, 40, 41) that antibody constant and variable domains influence each other. We further showed that the Fc-effector function was, irrespective of the original subclass, most potent in the IgG3 subclass. Therefore, future work with subclass-switched mAbs is warranted to broaden our understanding of variable and constant domain interactions and how that influences immune function in particular diseases.

Overall, this study highlights the benefit of subclass-switching mAbs to IgG3 and using them in oligoclonal cocktails for enhancing in vitro opsonic function. These results are important for the future development of therapeutic mAbs when Fc- and CR-mediated phagocytosis is desirable. In the context of SARS-CoV-2 and its VOCs, using opsonic monoclonal therapeutics could constitute a promising avenue for further research, especially since they are less dependent on binding to mutation-prone epitopes in the RBD. Our study shows the promise of using nonneutralizing but opsonic mAbs against SARS-CoV-2 infections and using IgG3 mAbs instead of IgG1s due to their potent Fc-effector functions. The differences between our in vitro data with human phagocytes and animal outcomes stress the importance of future work on optimizing preclinical models for the therapeutic development of mAbs. Additionally, the study presented here is a reminder of the intricacies involved in B cell subclass switching and highlights the importance of different subclasses in an immune response.

Materials and Methods

IgG3 Plasmid Generation, Production, and Sequencing. The anti-spike mAbs used in this work were made from spike-reactive B cells from convalescent patients who were infected 6 wk earlier with SARS-CoV-2 (verified in the clinic) (5). Briefly, the V(D)J coding sequences from spike-reactive B cells were generated using 10× Genomics. The variable regions were cloned into pTwist IgG1 vectors (Twist Biosciences) containing the IgG1 constant heavy domain. The plasmid containing the constant heavy domain gene for IgG3 was produced previously. The exchanging of the heavy chain constant domains was done by PCR of the IgG1 vector backbone and the IgG3 constant region to replace the IgG1-specific domain. For details, see *SI Appendix, Materials and Methods*.

Cell Culture and Antibody Production. Antibodies were produced in Expi293F suspension cells in Expi293 medium (Gibco). Transfection with heavy and light chain plasmids was carried out using the Expifectamine293 kit (Gibco) according to the manufacturer's instructions. In order to capture the IgGs from the medium, protein G sepharose 4 Fast Flow (Cytiva) was used. The concentration and quality of the purified antibodies were spectrophotometrically measured with the IgG setting of the Nanodrop (Denovix) as well as subjecting the antibodies to an SDS-PAGE and comparing the band intensity to a serial dilution of Xolair (Omalizumab). For details, see *SI Appendix, Materials and Methods*.

Generation of Spike-Coated Beads. Spike protein was generated by transfecting Expi293F cells with 40 μg plasmid containing the gene for the spike protein (CS/PP spike encoding a secretable version of the protein was used to allow purification from cell culture supernatants), donated previously to us by Dr. Florian Krammer's lab (5). Then, 200 μg spike protein was biotinylated according to the instructions of the EZ-LinkTM Micro Sulfo-NHS-LCBiotinylation Kit (ThermoFisher). Then, 500 μL (5×10^7 million beads) of fluorescent (APC) streptavidin microsphere beads (1 μm, Bangs Laboratories) were conjugated with the biotinylated spike protein (200 μg) according to the manufacturer's instructions.

Flow Cytometry-Based Avidity Measurements. The binding assays were performed in a 96-well plate which had been precoated with 200 μL of 2% BSA (in phosphate-buffered saline (PBS)) overnight at 4 °C. Then, 100,000 spike-coated beads were used in all wells, with antibody concentrations ranging between 0.02 and 0.2 to 2 μg per mL. The beads were opsonized at a volume of 100 μL in 1× PBS at 37 °C for 30 min on a shaking heat block. The wells were washed twice with PBS. To assess antibody binding to spike beads, 50 μL of (1:500 diluted) a Fab-specific fluorescent secondary antibody (#109-546-097, Jackson ImmunoResearch) was used to create a fluorescent signal. The secondary antibody was left to incubate with the spike-bead antibody complex at 37 °Cs for 30 min on a shaking heat block. Then, 100 μL of PBS was added to the wells before analysis in the flow cytometer. The beads were analyzed using a Beckman Coulter Cytoflex flow cytometer. For details, see *SI Appendix, Materials and Methods*.

SPR Kinetic Assay. To study antibody binding kinetics to the spike trimer, RBD, or NTD, we immobilized a high-capacity amine sensor chip (Bruker) with Anti-human IgG (Fc) antibody (Cytiva BR-1008-39) at 25 μg/mL in 10 mM sodium acetate buffer pH 5 at flow rate 10 μL/min and contacting 300 s. This was done in a MASS-16 biosensor instrument (Bruker) with a running buffer consisting of PBS + 0.05 % Tween 20. For details, see *SI Appendix, Materials and Methods*.

ELISA Avidity Measurements. For ELISA, 1 μg/mL of spike protein in PBS was immobilized onto ELISA High-bind plates (Sarstedt) overnight at 4 °C. The wells were washed with PBST (1× PBS with 0.05 % Tween 20) 3 times and then blocked with 2% BSA/PBS for 1 h at room temperature. After three washes, a serial dilution of primary antibody (anti-spike mAb) was added (100 μL of mAbs with a concentration of 0.08 up to 20 μg/mL) and incubated for 1 h at room temperature. The wells were washed three times. A rabbit anti-human light chain-HRP secondary antibody (anti-kappa for clone 57, anti-lambda for clone 11 and 66) (Abcam ab202549 and ab200966) at a dilution of 1:5,000 in PBS was added and left to incubate for 1 h at room temperature. The wells were washed 3 more times with PBST. Finally, 100 μL developing reagent (20 mL sodium citrate pH 4.5 + 1 mL ABTS (2,2′-Azino-bis(3-ethylbenzothiazoline-6-sulfonic acid) diammonium salt, 0.2 g in 10 mL water, Sigma) + 0.4 mL 0.6% H_2O_2) was added. OD450 was recorded after 15 to 30 min. Data were plotted with GraphPad Prism.

C1q Deposition Assay. To study complement activation, we opsonized 500,000 spike beads with 0.1–1–10 μg/mL of mAbs with 1% antibody-depleted serum as a source for complement in a 96-well plate previously coated with 2% BSA. After 30 min of opsonization at 37 °Cs on a shaking heat block (300 RPM), the wells were washed 2 times with PBS before a FITC fluorescently labeled anti-C1q Ab was added (ab4223, Abcam) (1:250 dilution from stock, 50 μL). The anti-C1q Ab was left with the beads for 30 min at 37 °C on a shaking heat block (300 RPM). PBS was added to resuspend the beads in a final volume of 150 μL. The gate for spike beads was set based on forward and side scatter, and the gate for C1q deposition was set based on the results of the control-IgG1(*SI Appendix*, Fig. S5*A*). The data acquired were analyzed with Flowjo and plotted in GraphPad Prism. The EC_{50}-analysis was performed on GraphPad Prism using a nonlinear regression model with the bottom constrained to 0 and the top value constrained to 100% for the % beads-C1q deposition analysis. For the MFI EC_{50} analysis, the top was set to be shared and greater than 0.

Flow Cytometry-Based Phagocytosis Assays. Phagocytosis experiments were done with the same batch of spike beads used in the binding assay. To assess internalization, the red-fluorescent beads were stained with pHrodo green (P35369, ThermoFisher), a pH-sensitive dye using 5 μL of 10 mM of pHrodo green (ThermoFisher) in 95 μL of Na_2Co_3 (pH 9) for 30 min at 37 °Cs. Excess stain was washed away with PBS. THP-1 cells (Sigma-Aldrich) were cultured as described previously (5). Opsonization was performed for 30 min at 37 °C on a shaking heat block (300 RPM) in a volume of 100 μL. A gate for THP-1 cells was set up based on their forward and side scatter (*SI Appendix*, Fig. S4*A*). The gate for internalization and association was set with negative control of cells only (Fig. 3*A*). For details, see *SI Appendix, Materials and Methods*.

Monocytes were isolated from the blood of healthy donors first by acquiring a PBMC layer by using Polymorphoprep (Abbot). Monocytes were purified from the PBMC layer through positive selection using CD14 Microbeads (Cat#130-050-201, Miltenyi Biotec) according to the manufacturer's instructions. Following isolation, monocytes were counted using an XN-350 hematology analyser (Sysmex). Neutrophils were, in turn, isolated with Polymorphprep gradient according to the manufacturer's instructions and were counted with a Bürker chamber. Isolated cells were kept on ice for 1 h after being resuspended in sodium media and adjusted to 2×10^6 cells/mL. Donors had given written and oral consent to participate in this study. They were provided oral information on the purpose of the donation, which was used only to isolate and use the monocytes and neutrophils in flow and microscopy experiments. This study protocol was approved by the Swedish ethical review authority (2020/01747).

For monocyte phagocytosis experiments, spike beads were opsonized with 10 μg/mL of mAbs (IgG control mAb or OctomAb IgG3) but without any serum. Monocytes were gated using size and granularity (*SI Appendix*, Fig. S6*A*). Further selection was made by gating for CD14-positive cells. For details, see *SI Appendix, Materials and Methods*.

For the neutrophil experiments, the spike beads were opsonized with 10 μg/mL of mAbs with 1% antibody-depleted serum (Pel-Freeze, Cat#34014-10) for 30 min at 37 °C on a shaking heat block (300 RPM) (100 μL final volume). To only study the effects of Fc-mediated phagocytosis, we heat-inactivated the serum at 56 °C for 1 h. Both the heat-inactivated serum and normal human serum were added to the respective wells. A gate was set for FSC-A and SSC-A to mark the neutrophils (*SI Appendix*, Fig. S6*B*). This population was further selected for by the CD18 marker (*SI Appendix*, Fig. S6*B*). For details, see *SI Appendix, Materials and Methods*.

IgG mAb Aggregation Quality Control Experiments. After production and purification of the mAbs, we performed a quality control of the mAbs to test whether aggregation could influence the results. The results from this quality control can be found in *SI Appendix*, Fig. S4*C*. For details, see *SI Appendix, Materials and Methods*.

Live Imaging Phagocytosis Assay.*Cell preparation and spike bead opsonization.* Neutrophils were isolated from 4 healthy donors through Polymorphprep as described above. The cells were then left on ice for 1 h in aliquots of 2×10^6/mL per donor. Cells were seeded on an 8-well Ibidi-plate (Cat#80827, Ibidi GmbH, Germany) at a density of 1×10^5 cells/well for 1 h with 5% CO_2 at 37 °C. All Ibidi-plates were precoated with 3.3 μg/mL human fibronectin (F0895-1MG, Sigma) diluted in PBS. After the incubation, the cells were stained with Hoechst 1:20,000 (ThermoFisher, Germany) and Alexa Fluor 594-conjugated wheat germ

agglutinin (WGA) 1:333 diluted in sodium medium to a final volume of 300 µL/well. The excess stain was washed 3 times with 300 µL/well of sodium medium, before 250 µL/well of sodium medium was added.

Spike-biotinylated beads were prestained with pHrodo green prior to opsonization with 10 µg/mL antibodies (IgG3 OctomAb, IgG1 OctomAb, Ab94 IgG3, Control-IgG1) and 1% antibody-depleted serum (Pel-Freeze, Cat#34014-10). Beads were opsonized in 100 µL (containing 1×10^6 beads) for 30 min at 37 °C shaking heat block. After opsonization, 5×10^5 beads/well (50 µL) were added right before the initiation of live imaging to the previously seeded neutrophils.

Live fluorescence imaging and data acquisition. Time-lapse images of phagocytosis were recorded every 10 min for 60 min using a Nikon N-SIM microscope. For details, see *SI Appendix, Materials and Methods*.

Animal Experiment. Thirty-seven to 10-wk-old female K18 hACE2 (B6.Cg-Tg(K18-ACE2)2Prlmn/J) mice were split into 5 groups of 6 mice/group, and antibodies were administered in one single dose, intraperitoneally. Eight hours after antibody administration, animals were inoculated intranasally with 10^5 PFU of SARS-CoV-2 (Wuhan strain, isolate SARS-CoV-2/01/human/2020/SWE, sourced from the Public Health Agency of Sweden). The mice's body weights and health status were recorded daily, and the animals were killed if they lost more than 20% of their body weight or showed severe deterioration in health status. The infection proceeded for 10 d before the animals were killed. Blood, tissue, and BAL were harvested and stored accordingly. All the animal experiments were performed under the approval of the regional animal experimental ethics committee in Stockholm (2020 to 2021). BAL-fluid analysis for viral titers was analyzed as described previously using Qpcr (5).

Statistical Analysis. Statistical analysis was performed in GraphPad Prism. For comparisons between subclasses in specific clones or between mixes, a two-tailed *t* test was used for statistical analysis. When more than 2 treatments were analyzed, a one-way ANOVA with multiple comparisons test was used, with correction for multiple comparisons with Tukey's test.

Data, Materials, and Software Availability. All study data are included in the article and/or *SI Appendix*.

ACKNOWLEDGMENTS. We are grateful for funding from Vetenskapsrådet, Crafoord Foundation, Royal Physiographic Society, Alfred Österlund Foundation, Wallenberg Foundation, and Tanea Medical Ab.

Author affiliations: [a]Department of Clinical Sciences Lund, Division of Infection Medicine, Faculty of Medicine, Lund University, 221 84 Lund, Sweden; [b]Department of Immunotechnology, Faculty of Engineering, Lund University, 221 00 Lund, Sweden; [c]Department of Clinical Sciences Lund, Division of Pediatrics, Faculty of Medicine, Lund University, 221 84 Lund, Sweden; [d]Wallenberg Center for Molecular Medicine, Faculty of Medicine, Lund University, 221 84 Lund, Sweden; [e]Department of Laboratory Medicine, Clinical Microbiology, Skåne University Hospital Lund, Lund University, 221 85 Lund, Sweden; [f]Department of Microbiology, National Veterinary Institute, 751 89 Uppsala, Sweden; [g]Department of Microbiology, Public Health Agency of Sweden, 171 82 Stockholm, Sweden; [h]Scantox A/S, 171 65 Stockholm, Sweden; [i]Tanea Medical AB, 751 83 Uppsala, Sweden; and [j]SciLifeLab Drug Discovery and Development, Lund University, 221 00 Lund, Sweden

1. B. Hu, H. Guo, P. Zhou, Z. L. Shi, Characteristics of SARS-CoV-2 and COVID-19. *Nat. Rev. Microbiol.* **19**, 141–154 (2021).
2. P. Chen *et al.*, SARS-CoV-2 neutralizing antibody LY-CoV555 in outpatients with Covid-19. *N. Engl. J. Med.* **384**, 229–237 (2021).
3. M. A. Tortorici *et al.*, Ultrapotent human antibodies protect against SARS-CoV-2 challenge via multiple mechanisms. *Science* **370**, 950–957 (2020).
4. S. Yamayoshi *et al.*, Antibody titers against SARS-CoV-2 decline, but do not disappear for several months. *EClin. Med.* **32**, 100734 (2021).
5. W. Bahnan *et al.*, Spike-dependent opsonization indicates both dose-dependent inhibition of phagocytosis and that non-neutralizing antibodies can confer protection to SARS-CoV-2. *Front. Immunol.* **12**, 1–17 (2022).
6. E. S. Winkler *et al.*, Human neutralizing antibodies against SARS-CoV-2 require intact Fc effector functions for optimal therapeutic protection. *Cell* **184**, 1804–1820.e16 (2021).
7. I. Ullah *et al.*, Live imaging of SARS-CoV-2 infection in mice reveals that neutralizing antibodies require Fc function for optimal efficacy. *Immunity* **54**, 2143–2158.e15 (2021).
8. P. Kaplonek *et al.*, mRNA-1273 vaccine-induced antibodies maintain Fc effector functions across SARS-CoV-2 variants of concern. *Immunity* **55**, 355–365.e4 (2022).
9. G. Vidarsson, G. Dekkers, T. Rispens, IgG subclasses and allotypes: From structure to effector functions. *Front. Immunol.* **5**, 1–17 (2014).
10. M. Torres, A. Casadevall, The immunoglobulin constant region contributes to affinity and specificity. *Trends Immunol.* **29**, 91–97 (2008).
11. P. Bruhns *et al.*, Specificity and affinity of human Fcγ receptors and their polymorphic variants for human IgG subclasses. *Blood* **113**, 3716–3725 (2009).
12. B. Y. C. I. Bindon, G. Hale, M. Bruggemann, Human monoclonal IgG isotypes differ in complement activating function at the level of C4 as well as C1q. *J. Exp. Med.* **168**, 127–142 (1988).
13. S. Giuntini, D. C. Reason, D. M. Granoff, Combined roles of human IgG subclass, alternative complement pathway activation, and epitope density in the bactericidal activity of antibodies to meningococcal factor H binding protein. *Infect. Immun.* **80**, 187–194 (2012).
14. T. H. Chu *et al.*, Hinge length contributes to the phagocytic activity of HIV-specific IgG1 and IgG3 antibodies. *PLoS Pathog.* **16**, 1–25 (2020).
15. S. Foss *et al.*, Potent TRIM21 and complement-dependent intracellular antiviral immunity requires the IgG3 hinge. *Sci. Immunol.* **7**, eabj1640 (2022).
16. S. Kallolimath *et al.*, Highly active engineered IgG3 antibodies against SARS-CoV-2. *Proc. Natl. Acad. Sci. U. S. A.* **118**, 3–4 (2021).
17. T. de Neergaard, M. Sundwall, S. Wrighton, P. Nordenfelt, High-sensitivity assessment of phagocytosis by persistent association-based normalization. *J. Immunol.* **206**, 214–224 (2021).
18. M. Rabinovitch, Professional and non-professional phagocytes: An introduction. *Trends Cell Biol.* **5**, 85–87 (1995).
19. I. Ullah *et al.*, The Fc-effector function of COVID-19 convalescent plasma contributes to SARS-CoV-2 treatment efficacy in mice. *Cell Rep. Med.* **4**, 100893 (2023), 10.1016/j.xcrm.2022.100893.
20. R. Yamin *et al.*, Fc-engineered antibody therapeutics with improved anti-SARS-CoV-2 efficacy. *Nature* **599**, 465–470 (2021).
21. E. Winkler *et al.*, Human neutralizing antibodies against SARS-CoV-2 require intact Fc effector functions for optimal therapeutic protection. *Cell.* **184**, 1804–1820.e16 (2021), 10.1016/j.cell.2021.02.026.
22. G. Beaudoin-Bussières *et al.*, A Fc-enhanced NTD-binding non-neutralizing antibody delays virus spread and synergizes with a nAb to protect mice from lethal SARS-CoV-2 infection. *Cell Rep.* **38**, 110368 (2022).
23. L. A. VanBlargan *et al.*, An infectious SARS-CoV-2 B.1.1.529 Omicron virus escapes neutralization by therapeutic monoclonal antibodies. *Nat. Med.* **28**, 490–495 (2022).
24. W. T. Harvey *et al.*, SARS-CoV-2 variants, spike mutations and immune escape. *Nat. Rev. Microbiol.* **19**, 409–424 (2021).
25. H. Liu *et al.*, A combination of cross-neutralizing antibodies synergizes to prevent SARS-CoV-2 and SARS-CoV pseudovirus infection. *Cell Host. Microbe.* **29**, 806–818.e6 (2021).
26. V. Dussupt *et al.*, Low-dose in vivo protection and neutralization across SARS-CoV-2 variants by monoclonal antibody combinations. *Nat. Immunol.* **22**, 1503–1514 (2021).
27. S. Radaev, P. Sun, Recognition of immunoglobulins by Fcγ receptors. *Mol. Immunol.* **38**, 1073–1083 (2002).
28. J. M. Woof, D. R. Burton, Human antibody-Fc receptor interactions illuminated by crystal structures. *Nat. Rev. Immunol.* **4**, 89–99 (2004).
29. D. Yang, R. Kroe-Barrett, S. Singh, C. J. Roberts, T. M. Laue, IgG cooperativity–Is there allostery? Implications for antibody functions and therapeutic antibody development*MAbs* **9**, 1231–1252 (2017).
30. C. A. Diebolder *et al.*, Complement is activated by IgG hexamers assembled at the cell surface. *Science* **343**, 1260–1263 (2014).
31. P. Nordenfelt, H. Tapper, Phagosome dynamics during phagocytosis by neutrophils. *J. Leukoc. Biol.* **90**, 271–284 (2011).
32. N. Stapleton M., *et al.*, Competition for FcRn-mediated transport gives rise to short half-life of human IgG3 and offers therapeutic potential. *Nat. Commun.* **2**, 599 (2011).
33. S. Ko *et al.*, An Fc variant with two mutations confers prolonged serum half-life and enhanced effector functions on IgG antibodies. *Exp. Mol. Med.* **54**, 1850–1861 (2022), 10.1038/s12276-022-00870-5.
34. R. Bazin *et al.*, Use of hu-IgG-SCID mice to evaluate the in vivo stability of human monoclonal IgG antibodies. *J Immunol Methods* **172**, 209–217 (1994), 10.1016/0022-1759(94)90108-2.
35. B. Pierre, Properties of mouse and human IgG receptors and their contribution to disease models. *Blood* **119**, 5640–5649 (2012), 10.1182/blood-2012-01-380121.
36. D. Gillian, Affinity of human IgG subclasses to mouse Fc gamma receptors. *mAbs* **9**, 767–773 (2017), 10.1080/19420862.2017.1323159.
37. Z. Steplewski *et al.*, Biological activity of human-mouse IgG1, IgG2, IgG3, and IgG4 chimeric monoclonal antibodies with antitumor specificity. *Proc. Natl. Acad. Sci. U.S.A.* **85**, 4852–4856 (1988).
38. M. B. Overdijk, Crosstalk between human IgG isotypes and murine effector cells. *J. Immunol.* **189**, 3430–3438 (2012), 10.4049/jimmunol.1200356.
39. T. H. Chu, E. F. Patz, M. E. Ackerman, Coming together at the hinges: Therapeutic prospects of IgG3. *MAbs* **13**, 1882028 (2021).
40. A. Janda, E. Eryilmaz, A. Nakouzi, D. Cowburn, A. Casadevall, Variable region identical immunoglobulins differing in isotype express different paratopes. *J. Biol. Chem.* **287**, 35409–35417 (2012).
41. A. Janda, A. Bowen, N. S. Greenspan, A. Casadevall, Ig constant region effects on variable region structure and function. *Front. Microbiol.* **7**, 1–10 (2016).